Chapter 3

Emission mechanisms

3.1 Radiation of atoms and molecules

Bound-bound (energy quantized – line spectrum)

- **Absorption**
- **Emission**

Bound-free (continuum emission)

- **Ionization**

Free-bound (continuum emission)

- **Recombination**

Free-free (continuum emission)

- **Bremsstrahlung**

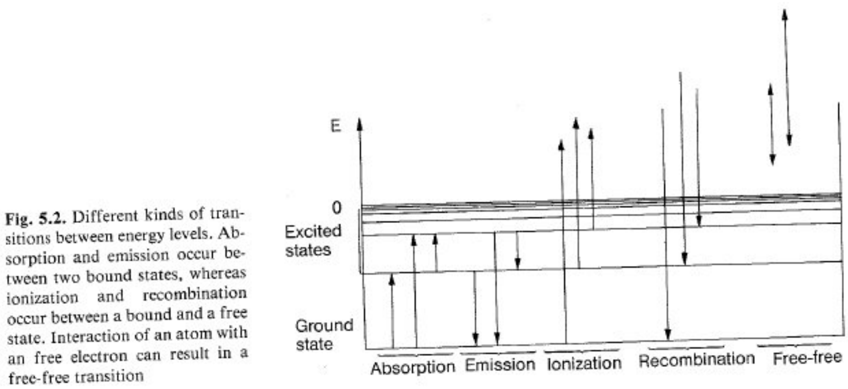

Figure 3.1: From Karttunen et al.: Fundamental Astronomy (Springer)

Spectral lines

- **Electron-positron annihilation (511 keV)** $e^+ + e^- \longrightarrow 2\gamma$
- **Neutron capture (2.22 MeV)** $^1H + n \longrightarrow {}^2H + \gamma$
- **De-excitation (radiative or collisional)**

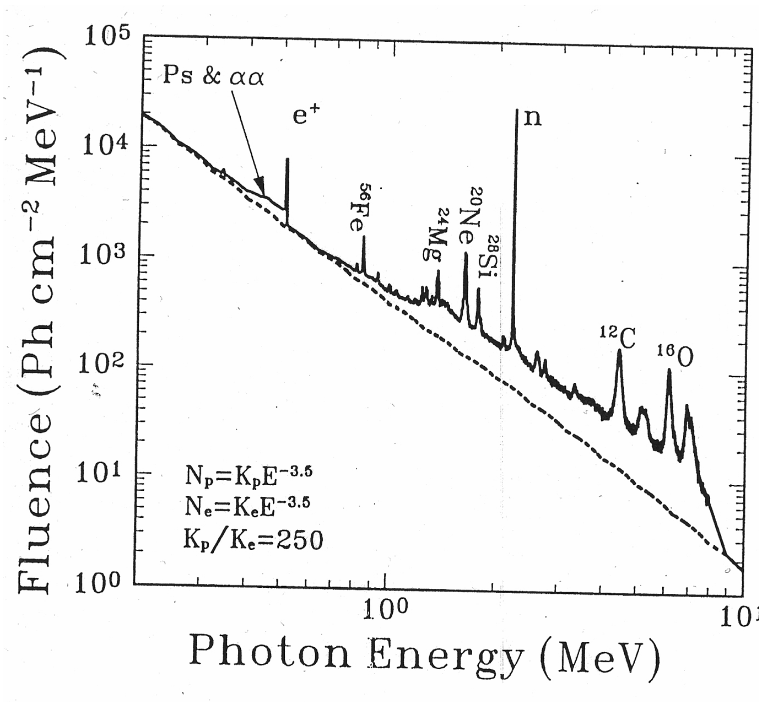

Figure 3.2: Neutron capture 2.223 MeV (delayed; attenuated near solar limb); e$^+$ annihilation 511 keV; De-excitation ^{16}O – 6.129 MeV; ^{12}C – 4.438 MeV; ^{20}Ne – 1.634 Mev etc.; Ps (positron continuum) + $\alpha\alpha$-interactions; Ions are due to accelerated particles (solar flares), break-up of He

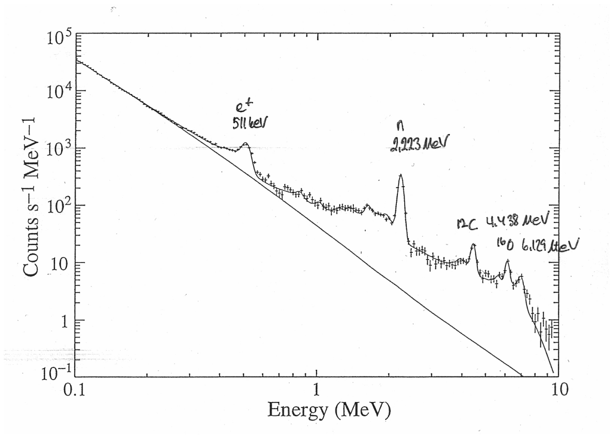

Figure 3.3: June 4, 1991 event: Radio flux at 80 GHz 140 000 sfu (1.4 billion Jansky)!

> 16 MeV	Date	Time (UT)	GOES Class	>50 keV	>300 keV	Narrow Lines >1 MeV	2.223 MeV
γ-rays	22-Nov-1998	6:39	X3.7	*	*		
	18-Aug-1998	22:16	X4.9	1830+/-21**	70+/-4**		
	29-May-1998	00:56	M6.7	916+/-15	13+/-1.5		
	08-May-1998	01:57	M3.1	398+/-4			
	01-Dec-1997	13:27	C6.6	<1			
	01-Dec-1997	2:34	M1.2	48.0+/-1.6			
	28-Nov-1997	5:02	M6.8	165.1+/-6.3			
	27-Nov-1997	16:13	C3.8	125.6+/-2.0			
*	27-Nov-1997	13:15	X2.6	680+/-34	25.2+/-4.1	1.2+/-0.6	1.2+/-0.3
	26-Nov-1997	18:32	M2.0	20.6+/-1.2			
	17-Nov-1997	15:05	C8.6	47.4+/-3.4			
	27-Oct-1991	13:15	X6.1	*	*	63+/-3	141+/-3
γ-rays	30-Jun-1991	2:56	M5.0	*	*	2.8+/-0.9	
* γ-rays and neutrons	04-Jun-1991	3:41	X12+	*	*	831+/-24	1050+/-19
neutrons	01-Jun-1991	15:05	X12+	+	+	+	+

Figure 3.4: CGRO-OSSE solar flare observations (previous solar max)

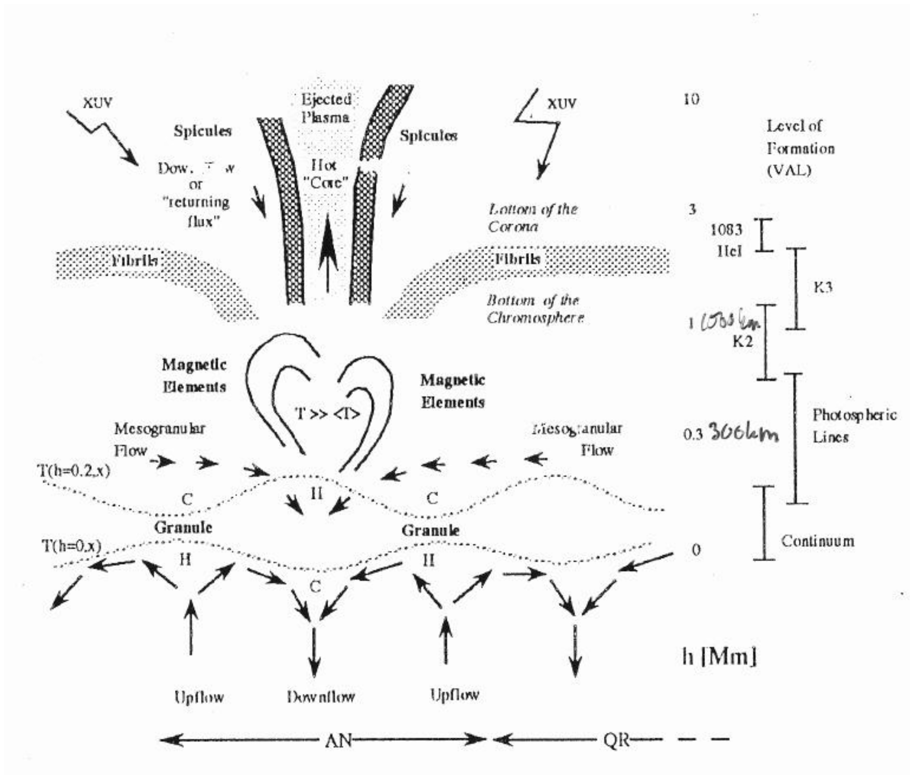

Figure 3.5: Formation heights of UV and EUV spectral lines

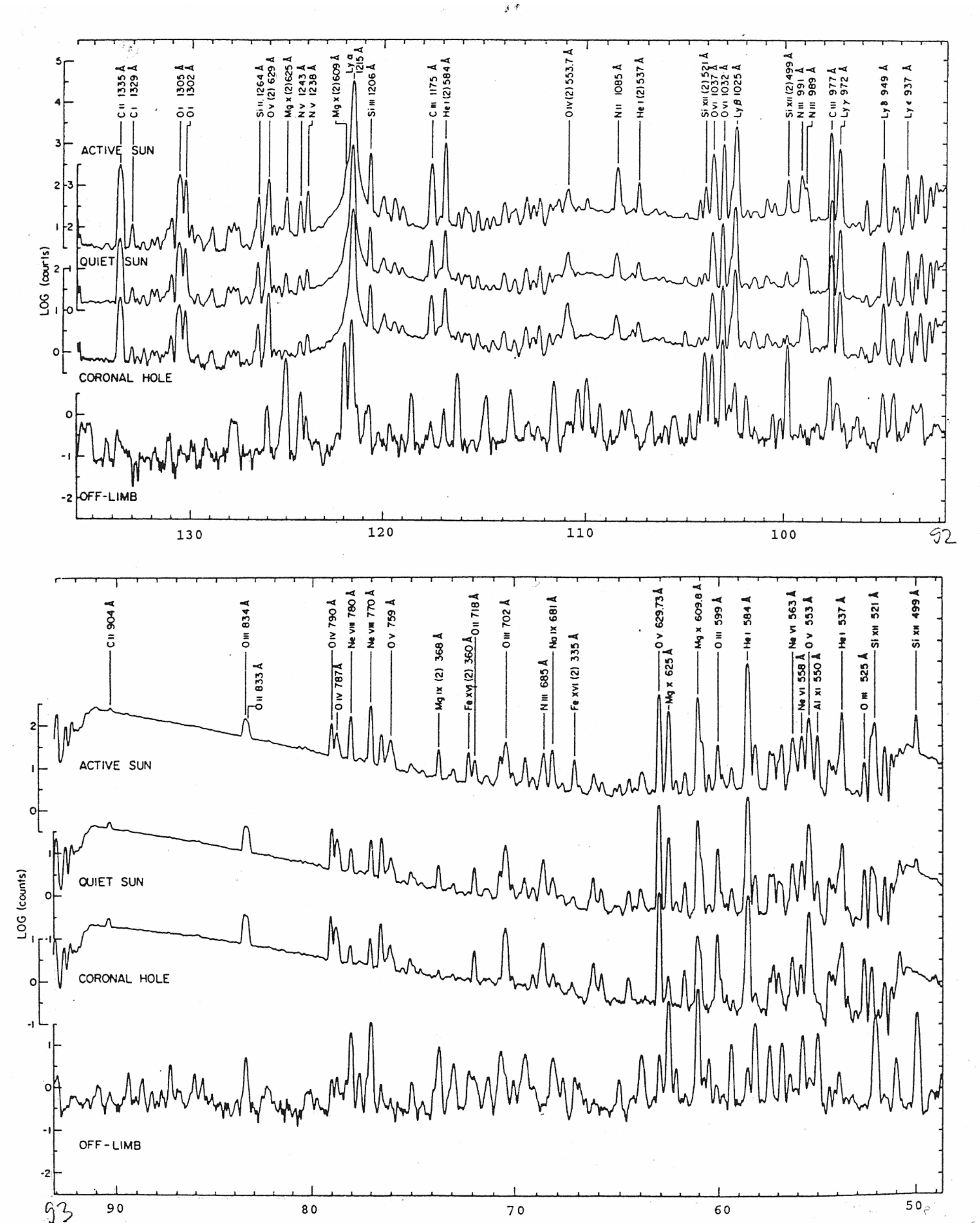

Figure 3.6: Solar spectra in far UV, Spacelab data (Vernazza & Reeves, 1978)

Plasma diagnostics with spectral lines

- **Line identification (CHIANTI database)**
- **Temperature T**, in K, from spectral fit
- **Emission measure EM**, in cm^{-3}, from spectral fit or filter ratio
- **Electron density N**, in cm^{-3}, $EM = \int_0^V N^2 \, dV = N^2 \, V$

Mason & Monsignori Fossi, Astron. Astrophys. Rev. 6 (1994), 123-179

Table 4.1. *Some prominent ultraviolet emission lines*

Wavelength (nm)	Identification	Temperature of formation (K)
17.1	Fe IX	900 000
17.48	Fe X	1 100 000
18.04	Fe XI	1 300 000
19.5	Fe XII	1 500 000
21.9	Fe XIV	1 800 000
23.4	Fe XV	2 000 000
24.9	Ni XVII	2 500 000
25.1	Fe XVI	2 200 000
25.6	He II	50 000
26.3	Fe XVI	2 200 000
26.5	Fe XIV	1 800 000
28.4	Fe XV	2 000 000
30.4	He II	50 000
33.5	Fe XVI	2 200 000
36.8	Mg IX	1 000 000
46.5	Ne VII	500 000
55.4	O IV	160 000
62.5	Mg X	1 100 000
99.7	C III	70 000
103.2	O VI	320 000
117.6	C III	70 000
120.6	Si III	30 000
121.5	H I[a]	20 000
124.0	N V	200 000
133.5	C II	20 000
139.4	Si IV	60 000
140.3	Si IV	60 000
153.3	Si II	14 000
155.0	C IV	110 000
164.0	He II	50 000
165.7	C I	$<$10 000
167.0	C I	$<$10 000
180.8	Si II	14 000
181.7	Si II	14 000

Note:
[a] Lyman-α of neutral hydrogen.

Figure 3.7: Table from K.J.H. Phillips, Guide to the Sun, Cambridge Univ. Press, 1992

3.2 Bremsstrahlung (free-free continuum emission)

- **Thermal bremsstrahlung**
- **Nonthermal bremsstrahlung**

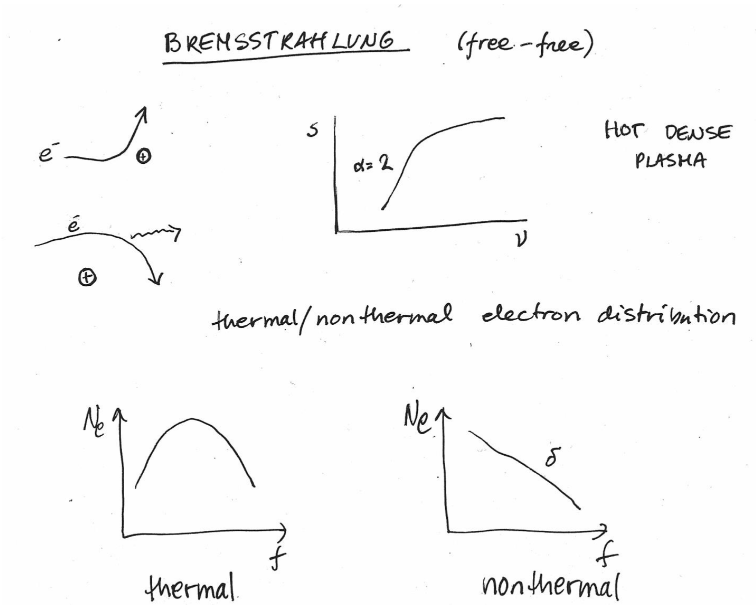

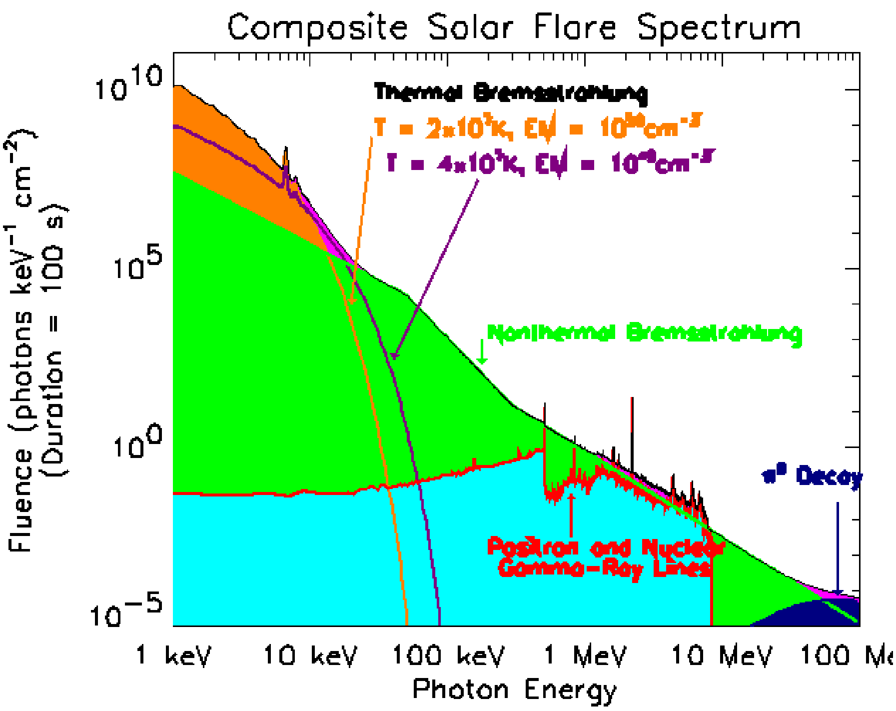

Figure 3.8: E = hc/λ, 1 keV = 12 Å; from RHESSI website

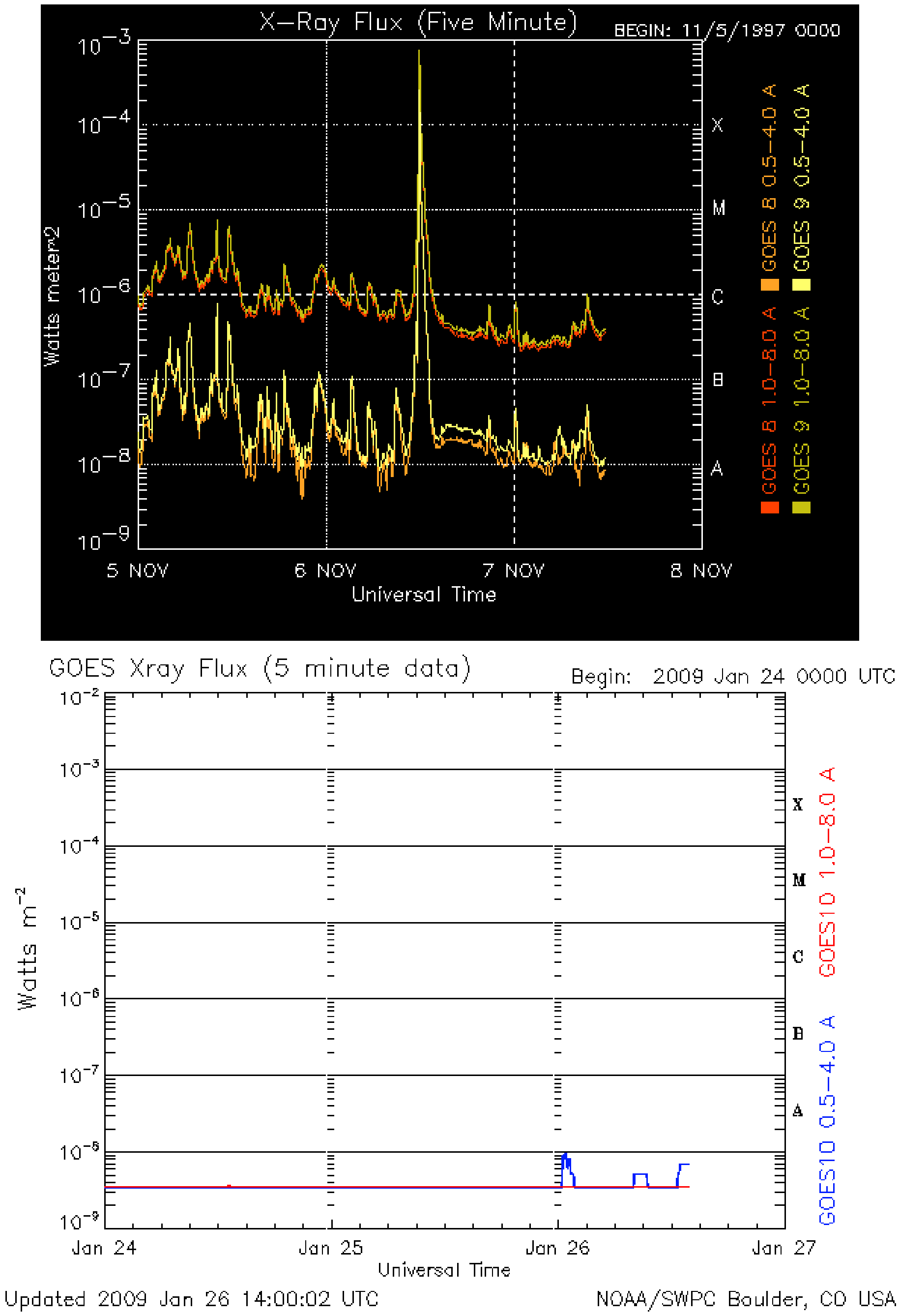

Figure 3.9: Thermal example: soft X-rays from the Sun. GOES satellites (1974–) are on geosynchronous orbits; 2-3 satellites cover 24 hours/day of continuous observations. Ion chamber detectors: $1-8$ Å($12-1.5$ keV) and $0.5-4$ Å($25-3$ keV). Flares are classified according to their flux: C, M, X classes. **Note that these are full disk observations – all events get detected and mixed if there are many happening at the same time!**

EXPRESSIONS TO DETERMINE TEMPERATURES AND EMISSION MEASURES FOR SOLAR X-RAY EVENTS FROM GOES MEASUREMENTS

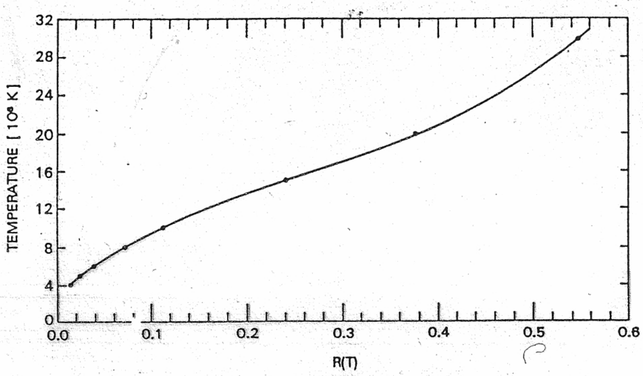

Fig. 3. Calculated points for the effective plasma temperatures as a function of detector ratios, and our analytic fit to them given by Equation (9).

NOAA - NGDC
GOES-satellite,
full sun

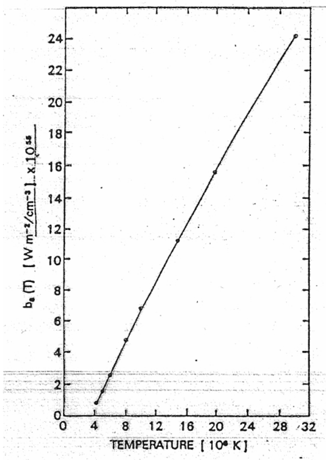

Fig. 4. Calculated points for the response per unit emission measure of the 1 to 8 Å GOES detector as a function of temperature of the emitting plasma. Our analytic fit to these points as given by Equation (10) is also shown.

$$R(T) = B_4/B_8 = b_4(T)/b_8(T)\,.$$

$$T(R) = 3.15 + 77.2R - 164R^2 + 205R^3\,,$$

$$10^{55}\,b_8(T) = -3.86 + 1.17T - 1.31\times10^{-2}\,T^2 + 1.78\times10^{-4}\,T^3$$

$$EM = B_8/b_8(T)\,.$$

$$EM = 10^{55}\,B_8/(10^{55}\,b_8(T))\,.$$

B_i - flux value above flare background

b_i - temperature dependent part of the detector's response

$B_8 = 1\text{-}8$ Å
$B_4 = 0.5\text{-}4$ Å

T - plasma temperature, 10^6 K

EM - emission measure, cm^{-3}

© Solar Phys. 95 (1985) 323-329

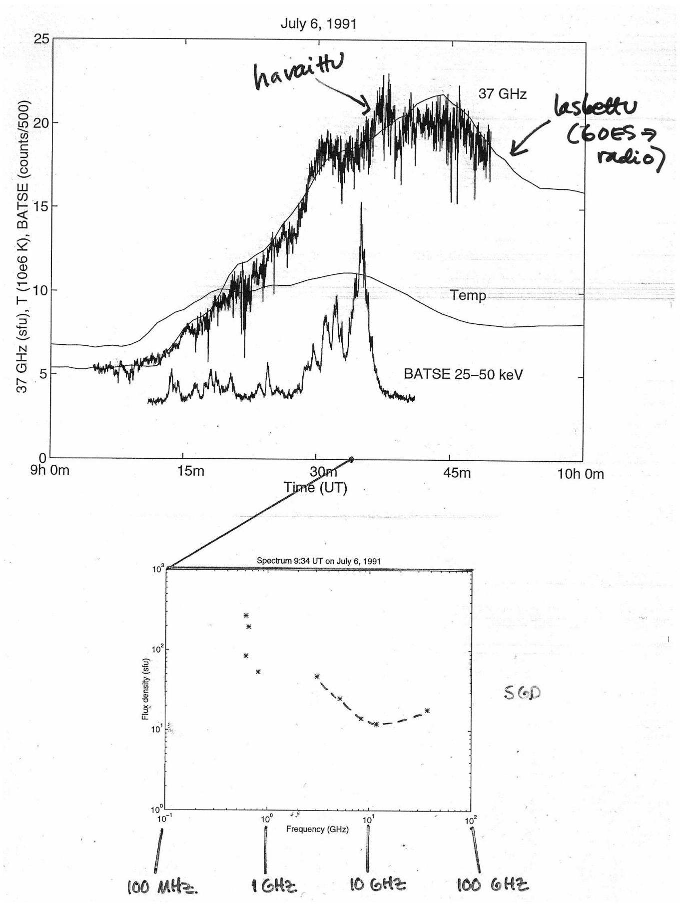

Figure 3.10: Gradual solar event: observed radio flux ('havaittu') and calculated radio flux ('laskettu') using the filter ratio from GOES X-rays.

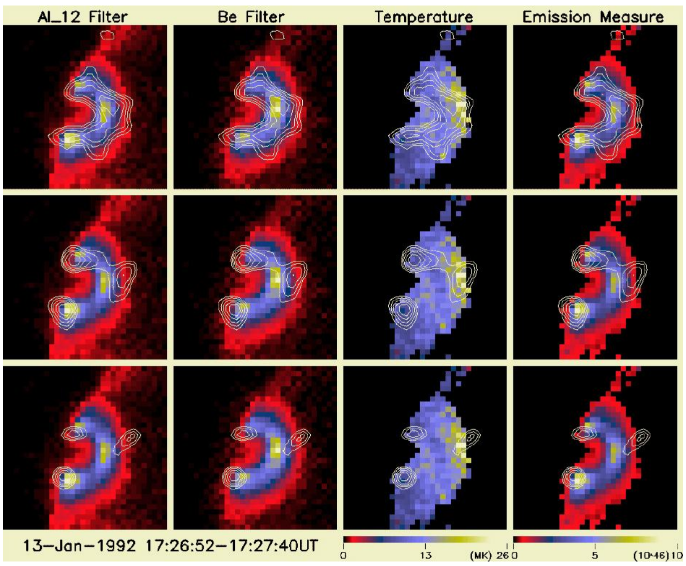

Figure 3.11: Masuda-flare: non-thermal source at the loop top? Loop is filled with hot plasma radiating in soft X-rays, with hard X-ray sources at loop footpoints (First Yohkoh results, 1992)

3.3 Gyroemission

The gyrofrequency ω_B for a particle with a charge q, mass m, and Lorentz factor γ, gyrating in a magnetic field B, pitch angle ψ being the angle between the B vector and the velocity vector, is in Gaussian units (Lang, 1980)

$$\omega_B = \frac{qB}{\gamma m c} \sin\psi \tag{3.1}$$

The gyrofrequency thus depends on the magnetic field strength B (in Gauss) and for non-relativistic electrons the gyrofrequency becomes

$$\nu_B = 2.8 \times 10^6 B \quad \text{(Hz)} \tag{3.2}$$

The particles gyrating in the magnetic field can have thermal or non-thermal velocity distributions. Emission can be classified as:

Gyroresonance(cyclotron) emission:

- non-relativistic ($\gamma = 1$) particles
- gyroresonance emission is concentrated at the fundamental frequency ($\omega = \Omega_e$) and at harmonics $s = \nu/\nu_B < 10$
- thermal electron distribution
- radiation is directed mainly along the magnetic field

Gyrosynchrotron emission:

- mildly relativistic ($\gamma <$ 2-3) particles
- gyrosynchrotron emission is strong at harmonic numbers $s = 10 < \nu/\nu_B < 100$
- both thermal and power-law electron distributions
- emission has a broad maximum perpendicular to the magnetic field

Synchrotron emission:

- relativistic particles
- broad continuum at high harmonics $s \sim (\gamma \sin\theta)^3$, i.e. near $\omega = \Omega_e \gamma^2 \sin\theta$
- power-law electron distributions only
- emission directed in the direction of instantaneous electron motion; peak of radiation perpendicular to the magnetic field

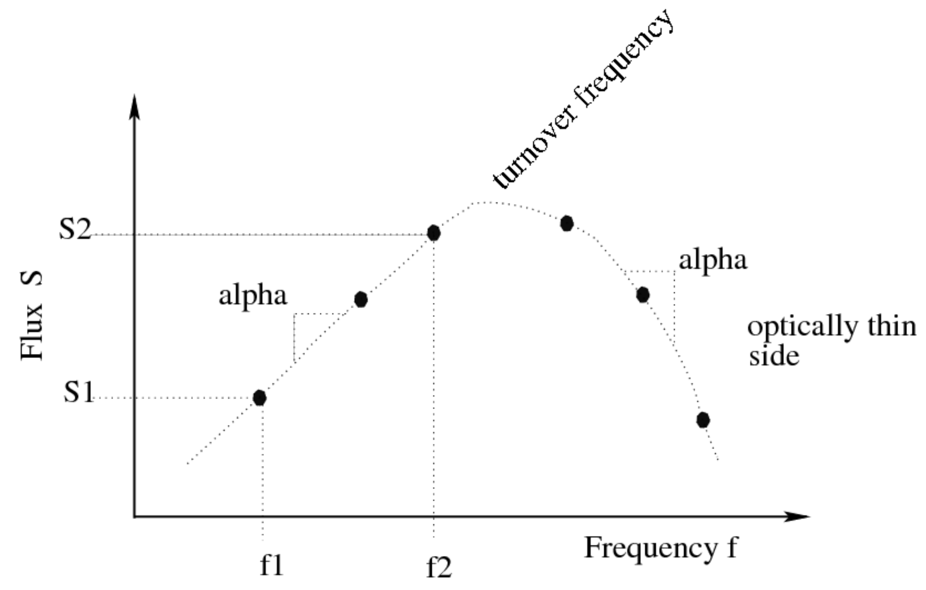

SPECTRAL INDEX alpha = $\frac{\log S2 - \log S1}{\log f2 - \log f1}$

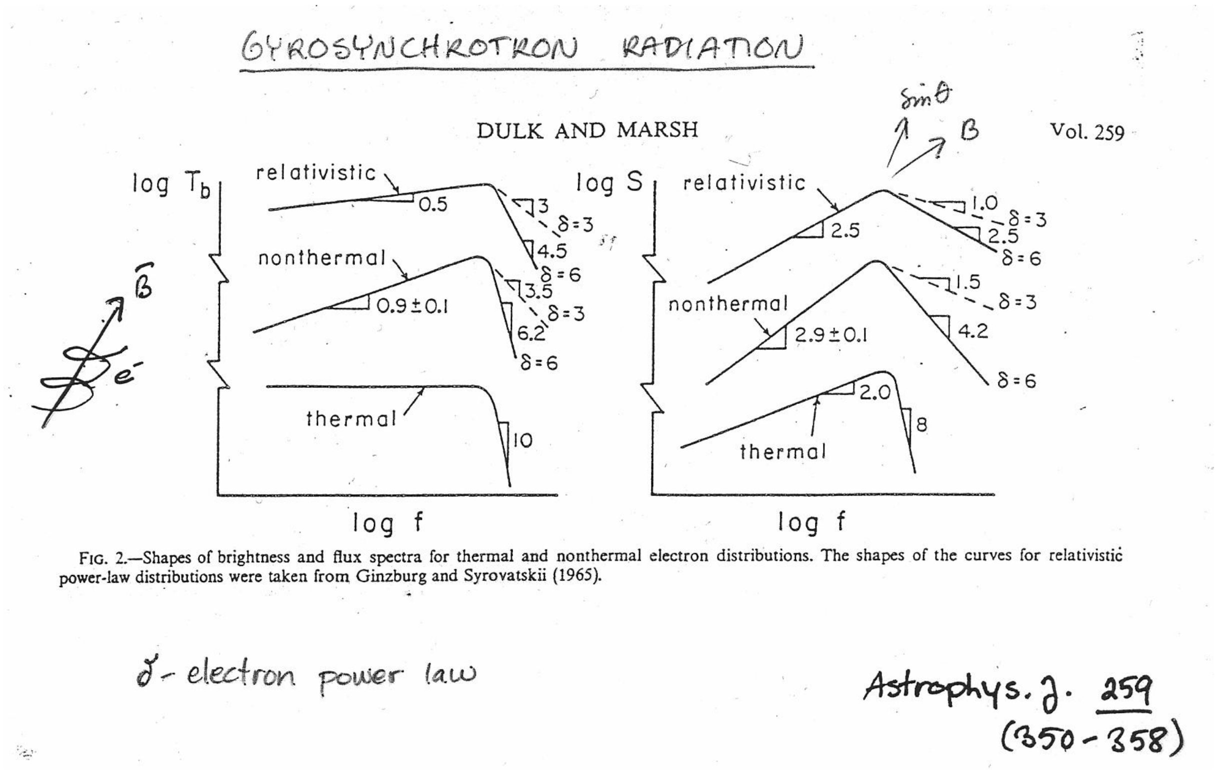

FIG. 2.—Shapes of brightness and flux spectra for thermal and nonthermal electron distributions. The shapes of the curves for relativistic power-law distributions were taken from Ginzburg and Syrovatskii (1965).

3.3.1 Gyrosynchrotron emission: mildly relativistic electrons

For optically thin ($\tau \ll 1$, $\nu > \nu_{peak}$) sources the radio flux density reduces to

$$S_\nu = \frac{2k\nu^2}{c^2} \int \tau \, T_{ef} \, d\Omega = \eta \, L \, \Omega \tag{3.3}$$

$$\eta \approx 3.3 \times 10^{-24}\, 10^{-0.52\delta}\, (\sin\theta)^{-0.43+0.65\delta} \left(\frac{\nu}{\nu_B}\right)^{1.22-0.90\delta} BN$$

where $d\Omega$ = source solid angle, L = source length along the line of sight, N = particle density. These approximations are valid for power-law indices $2 \le \delta \le 7$, viewing angles $\theta \ge 20°$, and harmonic numbers $\nu/\nu_B \ge 10$. The original calculations for gyrosynchrotron emission were presented by Ramaty (1969), and are now widely used because computers are more powerful!. These are simplified expressions by Dulk and Marsh (Astrophysical Journal, Vol. 259, 1982, p. 350-358).

There is a way to determine B in the corona, using radio observations:

$$\nu_{peak} \approx 2.72 \times 10^3\, 10^{0.27\delta}\, (\sin\theta)^{0.41+0.03\delta}\, (NL)^{0.32-0.03\delta}\, B^{0.68+0.03\delta} \tag{3.4}$$

But you then need δ (from spectral hard X-ray observations), NL and θ (from soft X-ray, EUV, and/or radio imaging)... Note: these are valid if the numbers are given in cgs units.

3.3.2 Gyrosynchrotron emission: thermal electrons

For thermal electrons with a Maxwellian energy distribution Dulk and Marsh present a simplified expression suitable for semiquantitative analytical modelling for the optically thin spectral region

$$S_\nu = \frac{2k\nu^2}{c^2} \int \tau\, T_{ef}\, d\Omega = \eta\, L\, \Omega \ , \ \ \eta \approx 60 \times 10^{-24} \left(\frac{\nu^8}{\nu_B^2}\right) T^8 \, \sin^6\theta\, B^{11}\, N\,. \tag{3.5}$$

The spectral peak of thermal gyrosynchrotron emission depends heavily on the plasma temperature and two expressions are given for different temperature ranges:

$$\nu_{peak} \approx 1.4\, (\frac{NL}{B})^{0.1}\, (\sin\theta)^{0.6}\, T^{0.7}\, B \quad (10^8 < T < 10^9\ K) \tag{3.6}$$

$$\nu_{peak} \approx 475\, (\frac{NL}{B})^{0.05}\, (\sin\theta)^{0.6}\, T^{0.5}\, B \quad (10^7 < T < 10^8\ K) \tag{3.7}$$

3.3.3 Synchrotron emission: ultrarelativistic electrons

In the case of ultrarelativistic electrons the emission is very strongly beamed in the direction of the electron motion and collisions are rare. The expressions for emissivity and peak frequency in the range $2 \le \delta \le 5$ can be written as

$$\eta \approx 8.6 \times 10^{-24} (\delta - 1) \sin\theta \left[\frac{0.175}{\sin\theta} \left(\frac{E_0}{1MeV}\right)^{-2} \frac{\nu}{\nu_B}\right]^{-(\delta-1)/2} BN\,, \tag{3.8}$$

$$\nu_{peak} \approx 3.2 \times 10^7\, \sin\theta \left(\frac{E_0}{1MeV}\right)^{(2\delta-2)/(\delta+4)} \tag{3.9}$$

$$\times \left[8.7 \times 10^{-12} \tfrac{\delta-1}{\sin\theta} NL\right]^{2/(\delta+4)} B^{(\delta+2)/(\delta+4)}$$

The emission occurs over a broad band centered at $\nu \approx \nu_B \gamma^2 \sin\theta/2$, i.e. at harmonic numbers $s \approx (\gamma \sin\theta)^3$.

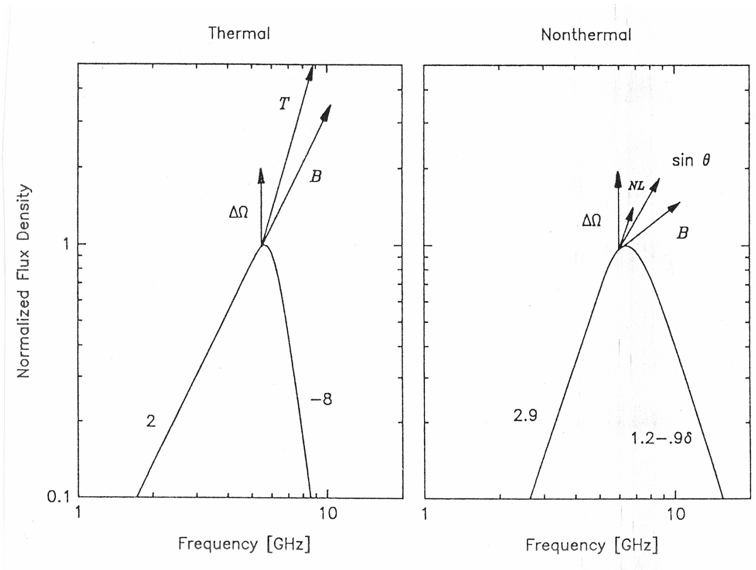

Figure 3.12: Parameters that change the spectral shape: temperature T, magnetic field strength B, source solid angle Ω, density × source length NL (along the line of sight), viewing angle $\sin\theta$. (From Stähli, Gary & Hurford, Solar Phys. 120, 1989)

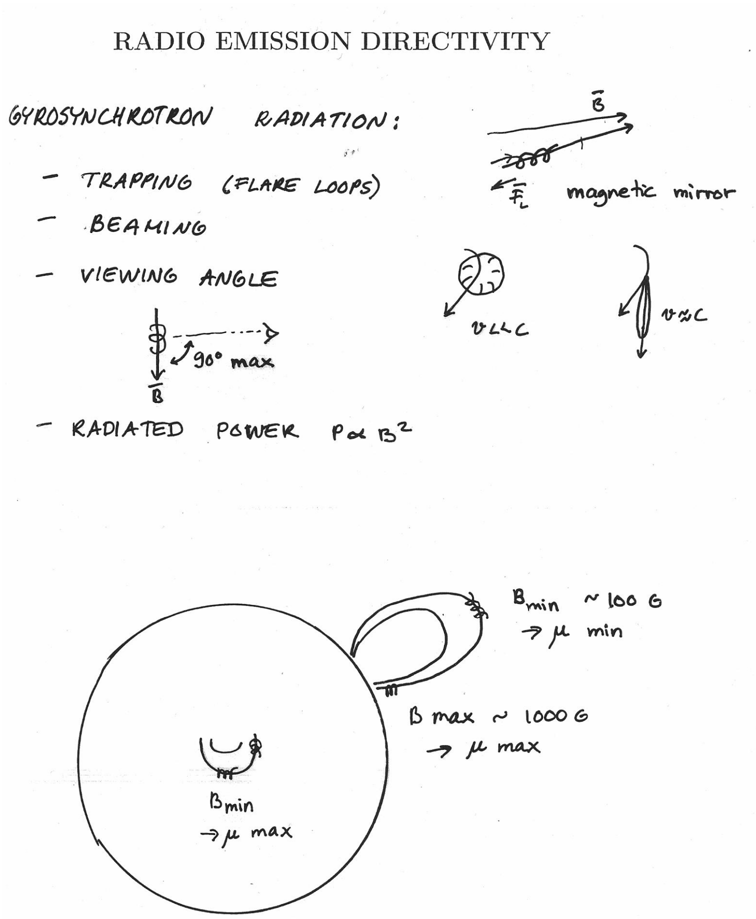

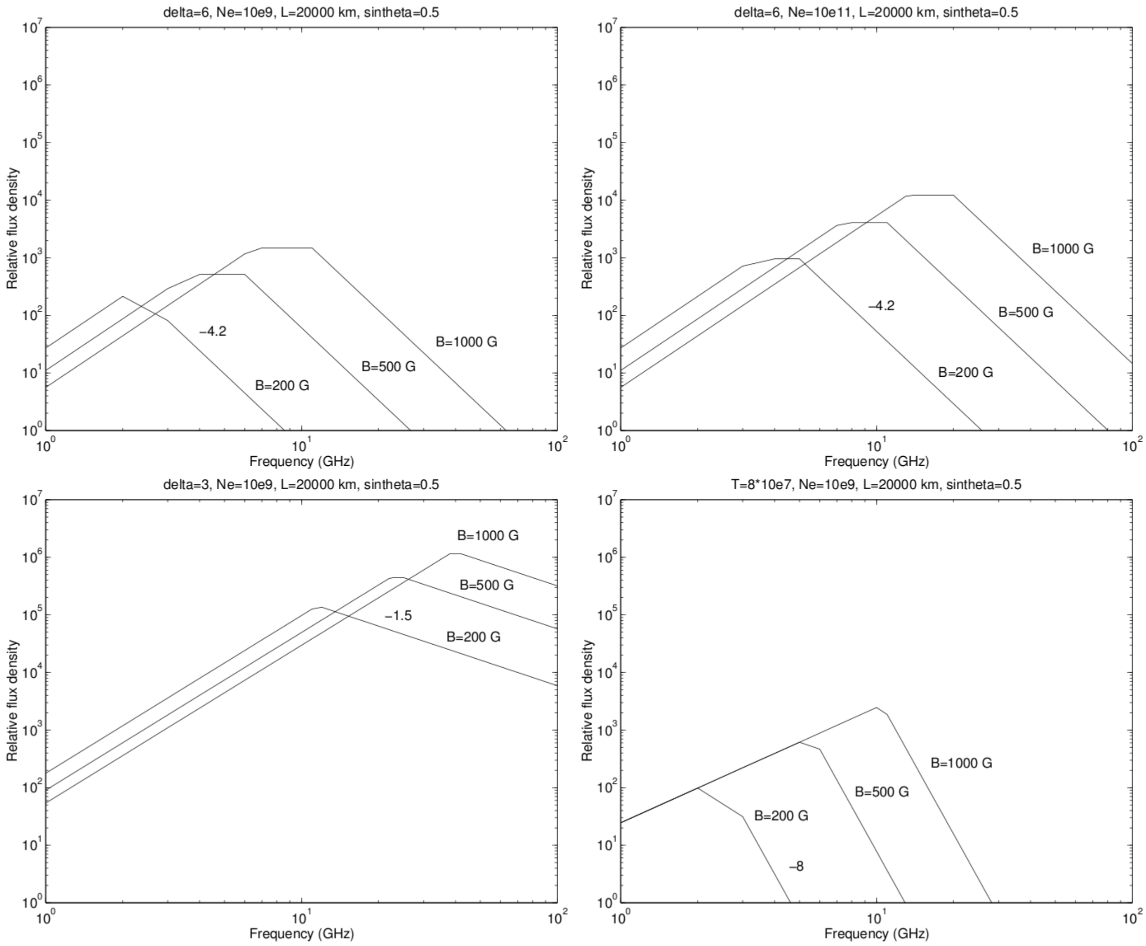

Figure 3.13: Examples of flux density spectra for gyrosynchrotron emission calculated from the given approximations, for magnetic field values of 200, 500, and 1000 Gauss. Path length L and viewing angle θ remain the same in all cases.

Top left:
flux density spectra for non-thermal gyrosynchrotron emission for $\delta = 6$, $N_e = 10^9$ cm^{-3}, $\theta = 30°$, L = 20 000 km

Top right:
otherwise similar to top left but now $N_e = 10^{11}$ cm^{-3} (electron density increased)

Bottom left:
otherwise similar to top left but now $\delta = 3$ (population of more energetic electrons present)

Bottom right:
flux density for thermal gyrosynchrotron emission, at plasma temperature $T_{ef} = 8 \times 10^7$ K

The figures show how an increasing magnetic field strength and a decreasing electron power law index move the spectral peak towards the higher frequencies, while changes in the source electron density alter the flux density, but do not change significantly the general spectral shape.

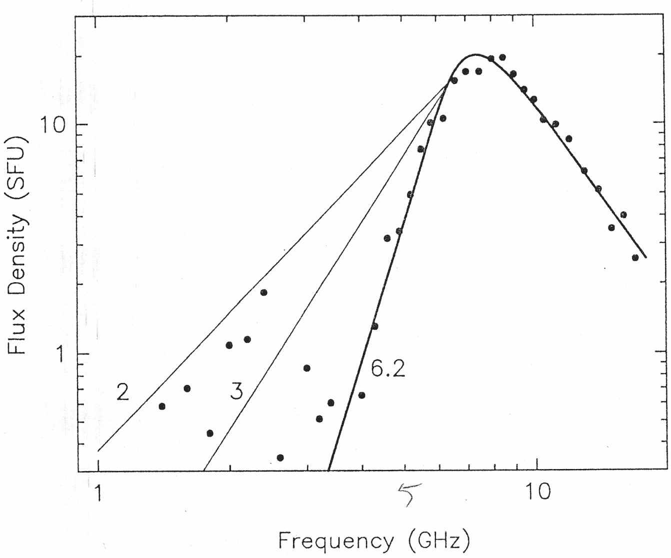

Fig. 8. Example of a spectrum with a steep low-frequency slope. The observed data points and the fit are shown together with the slopes expected from theory for a homogeneous source (about 2 for thermal and about 3 for nonthermal gyrosynchrotron emission).

Figure 3.14: Determining the spectral shape: especially at the optically thick side this can be difficult. A spectrum can always be a combination of several sources, at different T and N_e. This plot is made from Owens Valley observations, at several single frequencies between 1 and 18 GHz.

3.3.4 How to distinguish between bremsstrahlung and gyrosynchrotron emission?

- Thermal bremsstrahlung is only weakly polarized
- If plasma is isothermal and optically thick, polarization is zero
- Polarization in the optically thick side of gyrosynchrotron spectrum is extremely difficult to interprete
- On the optically thin side the degree of circular polarization in gyrosynchrotron emission is approximately 10...30%
- Polarization can be right (RCP) or left (LCP) handed and it can change during flare emission - depending on which end of the plasma loop electrons are gyrating
- Linear polarization has not been observed from the Sun (according to theory, it cannot propagate through the solar atmosphere)

3.4 Masers

Maser = amplification of radio waves by stimulated emission of radiation

Solar case for maser emission:
Electron cyclotron maser occurs when the resonance between electrons spiraling around a magnetic field and circularly polarised waves leads to growth of the waves.

The condition of growth is certain form of **anisotropy** → loss cone anisotropy at loop footpoint. Occurs at ν_B and second harmonic.

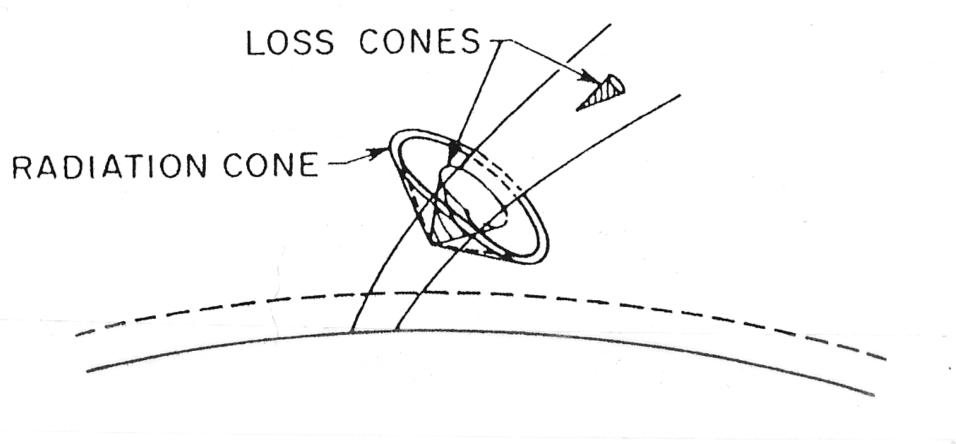

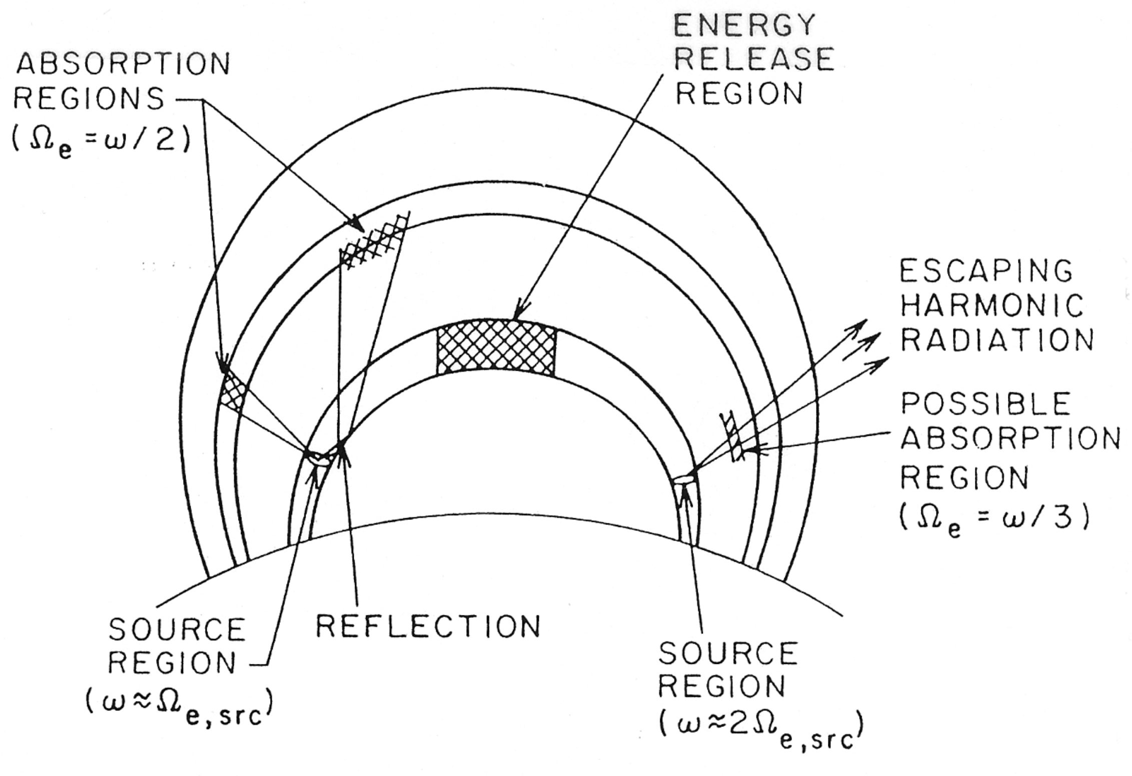

Figure 4 Schematic drawing of a sequence of magnetic flux tubes. At the top of a loop is a region where energy release is occurring. On the left is sketched a maser source region emitting at frequency $\omega = \Omega_e + \Delta$ at a location where the field strength is B_{src}. The cone of radiation is shown, including a reflection of the portion directed toward higher field strength; this radiation is reabsorbed at locations where $B = B_{src}/2$. At the right is sketched a maser operating at $2\Omega_e + \Delta$, perhaps being reabsorbed where $B = 2B_{src}/3$.

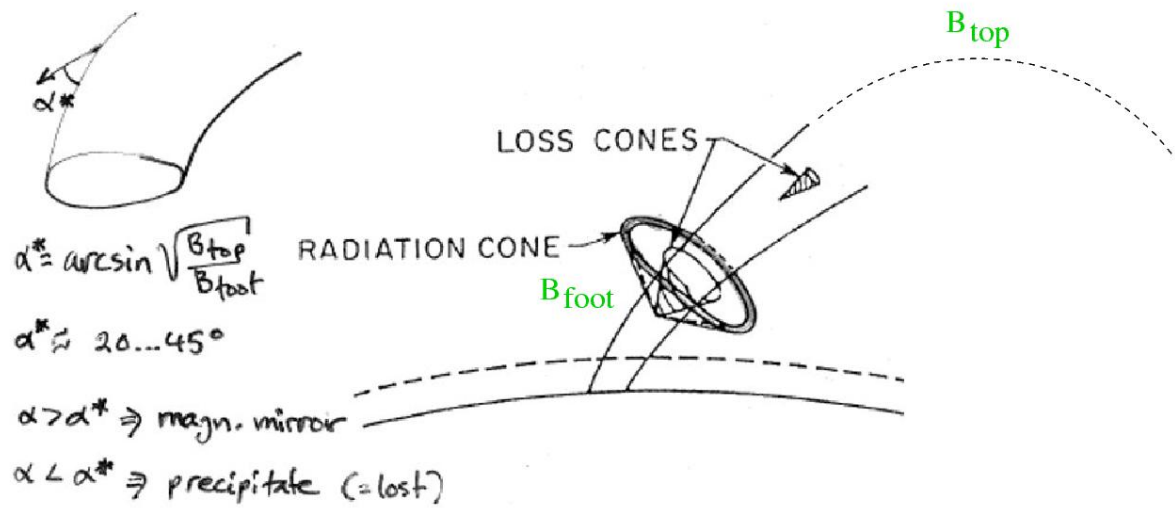

3.5 Absorption effects

Razin effect

The presence of a medium, tends to suppress synchrotron and gyrosynchrotron radiation at low frequencies. The Razin frequency ν_R in a plasma with an electron density N_e is defined as

$$\nu_R = \frac{20N_e}{B} = \frac{2\nu_p^2}{3\nu_B} \tag{3.10}$$

For ultra-relativistic electrons the suppression occurs at $\nu \leq \nu_R$ and for mildly relativistic and non-relativistic electrons at harmonics $s = \nu/\nu_B \leq \nu_p^2/\nu_B^2$ (Melrose, 1985; Dulk, 1985).

An illustrative example: in order to have Razin suppression effective up to 5 GHz, the electron density N_e (cm^{-3}) must be greater than $\sim 1.7 \times 10^8$ B. The required density is high even with the minimum expected magnetic field strength $B = 100$ G in the solar case.

Gyrosynchrotron self-absorption

Absorption by the population of radiating electrons itself. The process reguires a strong magnetic field and a high column density of electrons.

Free-free absorption

Collisional damping (free-free absorption) occurs when electrons begin to oscillate in resonance with the electric field and then collisions destroy the oscillation: the wave energy decreases and heats the plasma. Can happen when electromagnetic waves travel through cool dense structures in the solar atmosphere

Solar burst spectra

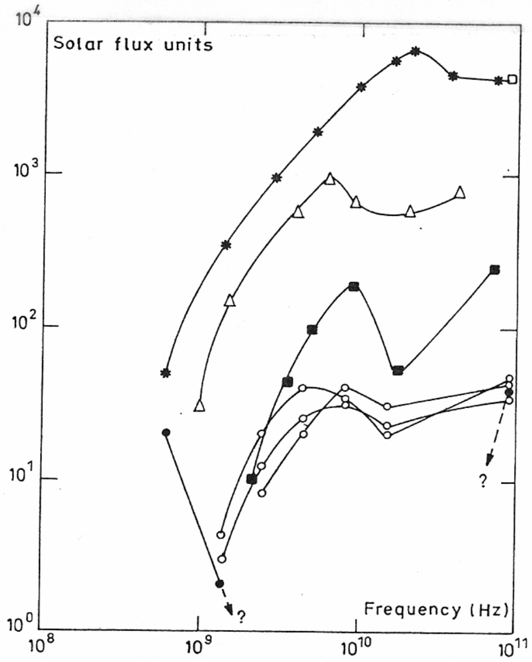

Fig. 3. Examples of solar burst spectra published in the literature, exhibiting a "flattening" towards mm-wavelengths or the superposition of a mm-wave spectral component. These results were obtained by the authors indicated is below. The measurements were taken with relatively poor time resolution and sensitivity. ∗ Croom (1970); □ Cogdell (1972); ○ Shimabukuro (1972); ● Shimabukuro (1970); ■ Akabane et al. (1973); △ Zirin and Tanaka (1973)

P. Kaufmann et al.: Synchrotron/inverse Compton solar burst emission

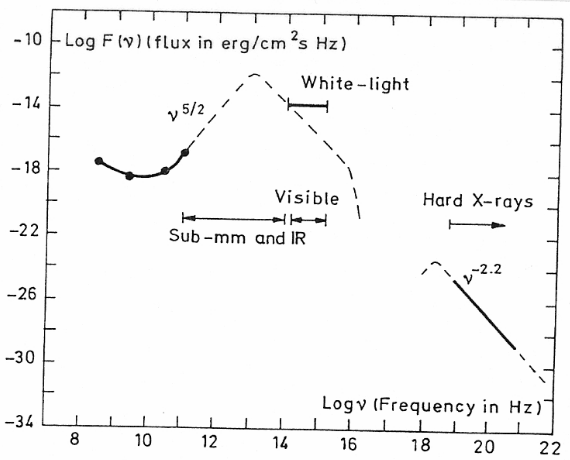

Fig. 4. The presently suggested interpretation associates the observed mm-wave spectrum (solid line for $\lambda \gtrsim 3$ mm) to a synchrotron spectrum peaking in the infrared range. Dashed lines are for a predicted qualitative spectrum at a time $t_0 < t < t_c$. The reported fluxes for white-light continuum in flares are close to the predicted synchrotron fluxes in the visible. Observed hard X-rays (solid line) are explained by inverse Compton quenching on the synchrotron produced photons, accounting for the short time scale durations ($\approx$60 ms)

Figure 3.15: Examples of peculiar radio spectra where flux rises towards the high frequencies (there is no spectral turnover around 10–20 GHz).

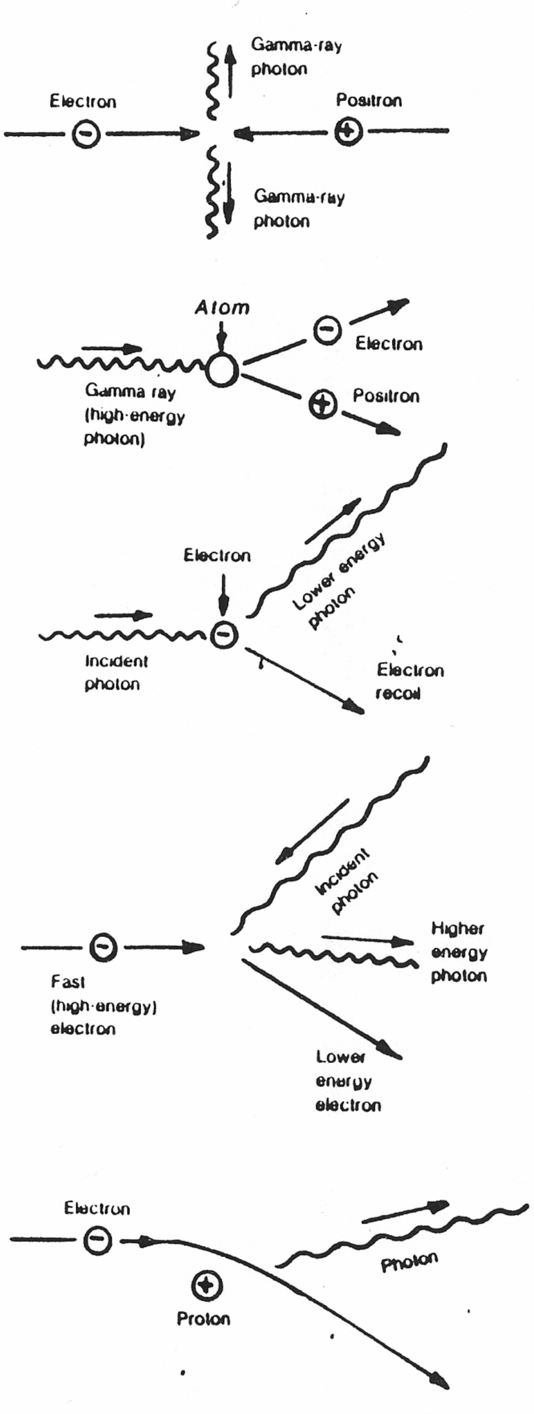

Matter into radiation. Annihilation of an electron-positron pair produces gamma-ray photons (511 000 electron volt line).

Radiation into matter. Photon transforms into an electron-positron pair on impact with atom. (Radiation into matter).

Compton scattering. Photon wavelength increased. Photon gives up some of its energy to electron. A Compton scattering event is a down-converter of the photon frequency.

Inverse Compton scattering. Photon wavelength decreased (light to x-ray or gamma ray). Electron gives up some of its energy to photon. An inverse Compton scattering event is an up-converter of photon frequency.

Bremsstrahlung. Free-free interaction of electron deflected by proton produces photon radiation. The electron leaving the interaction has less energy by the amount imparted to the photon. Typical radiation mechanism of an ionized hydrogen cloud.

Fig. 10-14. Some particle-particle and particle-photon interactions.

Figure 3.16: Inverse Compton scattering was proposed to be the reason for the peculiar radio spectra - but emission at microwaves should then be less.

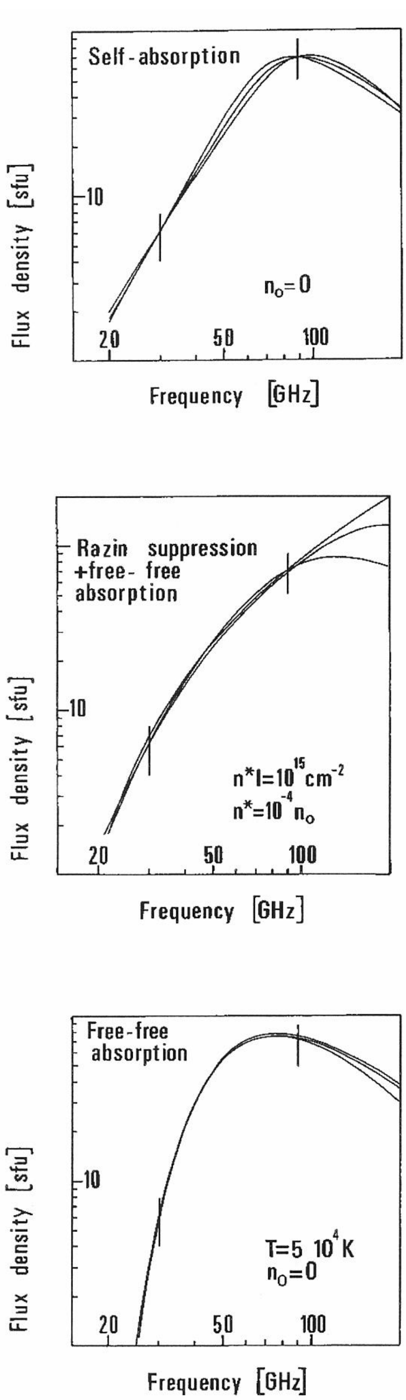

Fig. 4a–c. Gyrosynchrotron flux spectra computed for the mechanisms of absorption and suppression discussed in section 4 with the parameters of table 1 (1 sfu = $10^{-22}\,W\,m^{-2}\,Hz^{-1}$). Spectra are plotted for magnetic fields of 500 G, 1000 G and 2000 G (**a**), (**c**) and 250 G, 500 G and 1000 G (**b**) respectively. The vertical bars represent the observed flux densities at 30 and 90 GHz with an assumed error of 30%

outside the source of emission do not depend very much on the chosen parameters. This is different in the case where Razin suppression and free-free absorption inside the emissive source shape the spectrum: Most of the radiation above the spectral turnover frequency is then due to free-free emission, which is most intense at high electron densities and low temperatures.

In order to compare the numbers of energetic electrons in the microwave and the hard X-ray sources, we extrapolate the power-law spectrum (6) down to 10 keV and obtain the instantaneous number of nonthermal electrons at the peak of the microwave burst

$$N_\mu^*(10\,\mathrm{keV}) = 10^{32} - 10^{34}\,.$$

The number $N_x^*(10\,\mathrm{keV})$ of nonthermal electrons emitting hard X-rays through bremsstrahlung can be estimated from a power-law fit to the observed photon spectrum published by McClements and Brown (1986). With a spectral index of 3.2, Brown's (1971) Eq. 14, corrected by a factor π (Lin and Hudson, 1976), gives the instantaneous number

$$N_x^*(10\,\mathrm{keV}) = \frac{3\,10^{45}}{n_0}\,,$$

where n_0 is the density in the hard X-ray source in cm^{-3}. For densities above $10^{11}\,cm^{-3}$, the instantaneous numbers of nonthermal electrons in the microwave and hard X-ray sources are thus in a fairly good agreement. The electron lifetime of 60 ms and the total duration of the event of 20 s inferred from Kaufmann et al. (1985) give a total number of $3\,10^{34}$ to $3\,10^{36}$ electrons accelerated during the event to more than 10 keV, which represent an energy of 10^{27} to 10^{29} erg.

The close temporal association of microwaves and hard X-rays down to the limits of temporal resolution of the hard X-ray spectrometer (Kaufmann et al., 1985) and the quantitative agreement between the *instantaneous* numbers of electrons suggest that the emissions come from a common source. As the hard X-rays are most efficiently emitted in a medium with high density of ambient electrons, this indicates that the plasma in the high-frequency source may be sufficiently dense, cool and magnetized to affect the microwave radiation by Razin suppression, free-free absorption and self-absorption. Each of these mechanisms can act with different efficiency at different points of a magnetic loop. It is to be emphasized, however, that both the derived parameters and the steep observed spectrum favour a very compact source with a small amount of inhomogeneity. The decimetric observations show that some of the accelerated particles are not confined in this source, but escape into structures with density below $10^{10}\,cm^{-3}$. The absence of significant microwave radiation below 30 GHz requires that the escaping electrons be highly anisotropic or that their number be very small.

As an alternative explanation of the observations, free-free absorption outside the flaring loop requires a cool and dense structure between the loop and the observer. Radio maps at 35 GHz (Hachenberg et al., 1978) show that small-scale structures exist which are not optically thin to millimetre waves. Filaments absorb microwave radiation down to millimetre wavelengths (Raoult et al., 1979) and were shown long time ago to shield occasionally microwave emitting loops (cf. Kundu, 1965). Furthermore, Mouradian et al. (1983) showed that during flares cold arches rise into the solar atmosphere with parameters ($T = 10^4 - 5\,10^5$ K, $n_0 \sim 10^{11}\,cm^{-3}$) that can account for the efficient absorption of microwaves in the millimetre band. In the

Figure 3.17: Ludwig Klein (1987) proved with his calculations that different absorption mechanisms can change the spectral shape (decrease emission at microwaves so that at mm and sub-mm waves emission looks to increase) - no need for “exotic” emission mechanisms.

3.6 Plasma emission

$$\nu_p = \frac{q}{2\pi}\sqrt{\frac{N}{\epsilon_0 m}} \qquad \text{(Hz)} \tag{3.11}$$

where N is the particle density (m^{-3}), q is the charge of particle (C), m is the mass of particle (kg), and ϵ_0 is the permittivity of vacuum.

In the case of plasma with electron density N_e (m^{-3}) the plasma frequency becomes

$$\nu_p \approx 9\sqrt{N_e} \qquad \text{(Hz)} \tag{3.12}$$

An electron in an ionized gas is subjected to a linear displacement and it behaves as an oscillator with the characteristic plasma frequency ν_p. This disturbance is known as plasma oscillations or **Langmuir waves**

Radio emission can be produced by a two-stepped process, where electrostatic oscillations are first excited at or near the plasma frequency (e.g. by an energetic electron beam) and after that the Langmuir wave energy is converted to electromagnetic radiation via non-linear wave-wave interactions.

Plasma radiation occurs at or just above the plasma frequency ν_p and its second harmonic $2\nu_p$, but rarely if ever at higher harmonics.

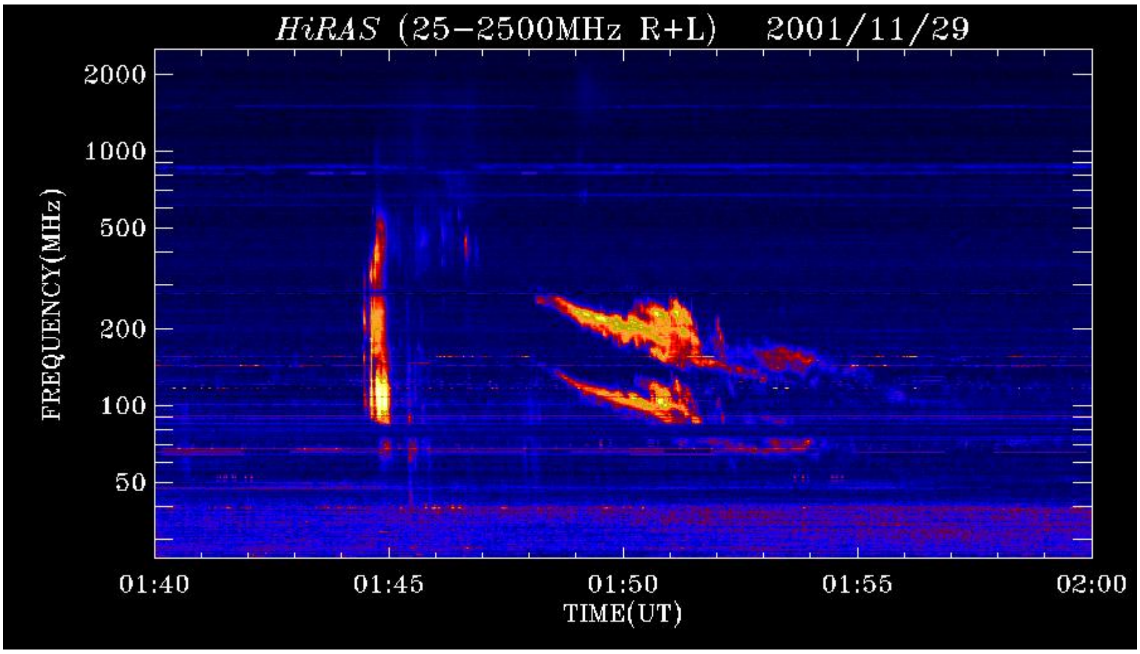

Figure 3.18: Radio dynamic spectrum at 25 MHz – 2 GHz. Plasma emission at the fundamental plasma frequency and its harmonic frequency (often called the 'second harmonic') are observed, frequency-drifting towards the lower frequencies (i.e., lower electron densities). The emission source speed is around 500–1000 km/s. A fast-drift structure in the spectrum is due to an electron beam, travelling at speed ~ 0.3c.

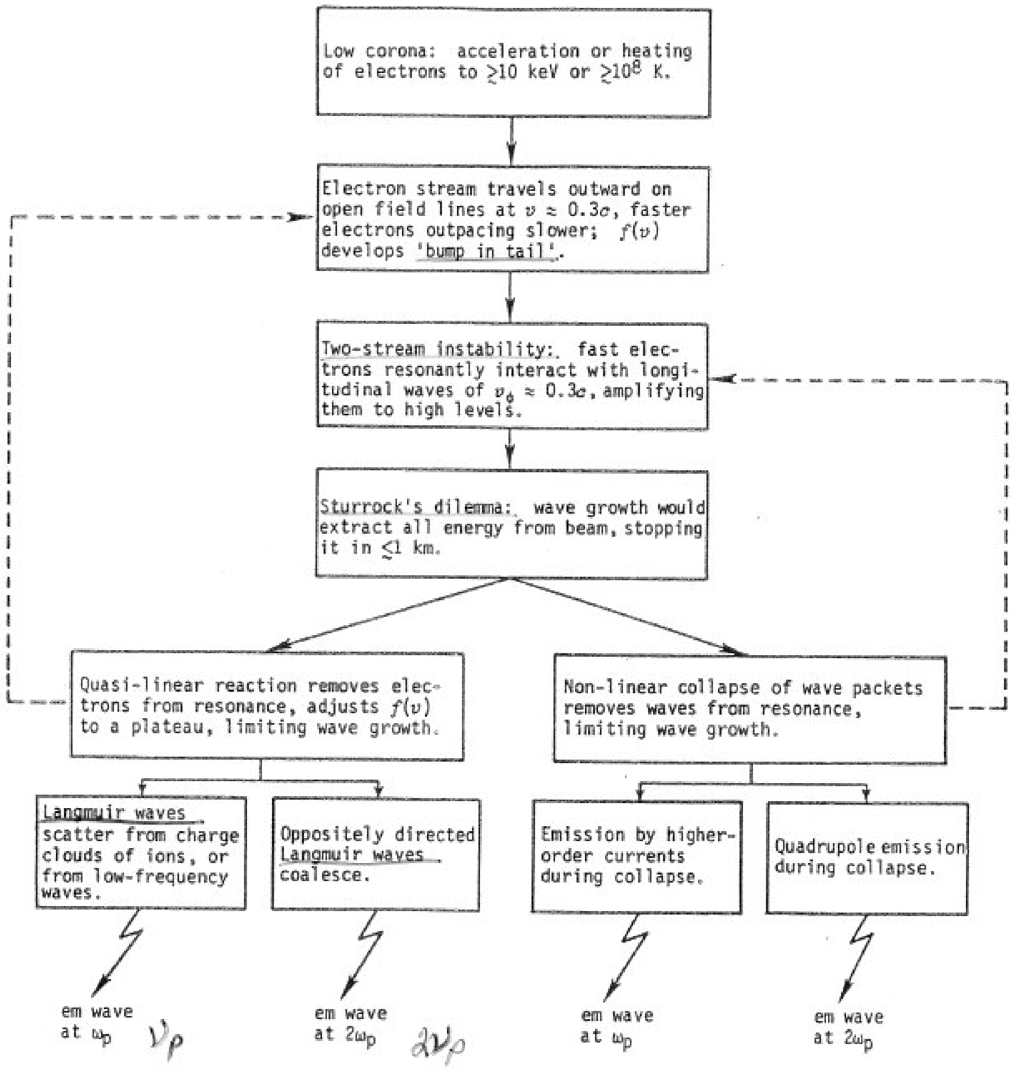

Fig. 8.1 - Steps in the theoretical description of emission of electromagnetic radiation by an electron stream in a plasma. The bottom half of the figure splits into two alternative theoretical lines of argument.

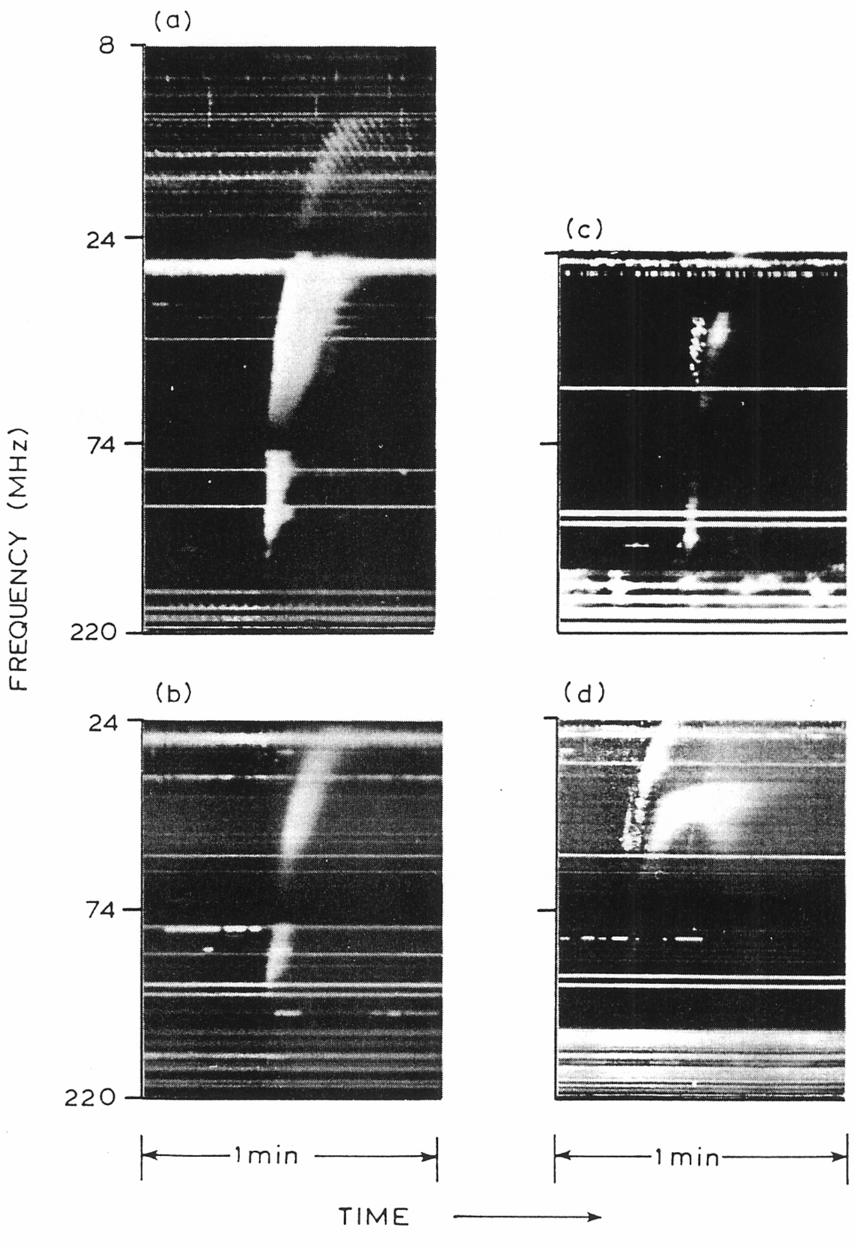

Fig. 12.1 - Dynamic spectra of several varieties of Type III bursts (examples from the Culgoora spectrograph records).
(a) Fundamental-harmonic pair, with 'ordinary' Type III bursts for both components (III-III pair).
(b) Structureless Type III burst.
(c) Type IIIb fundamental with smooth Type III harmonic (IIIb-III pair).
(d) Inverted-U burst.

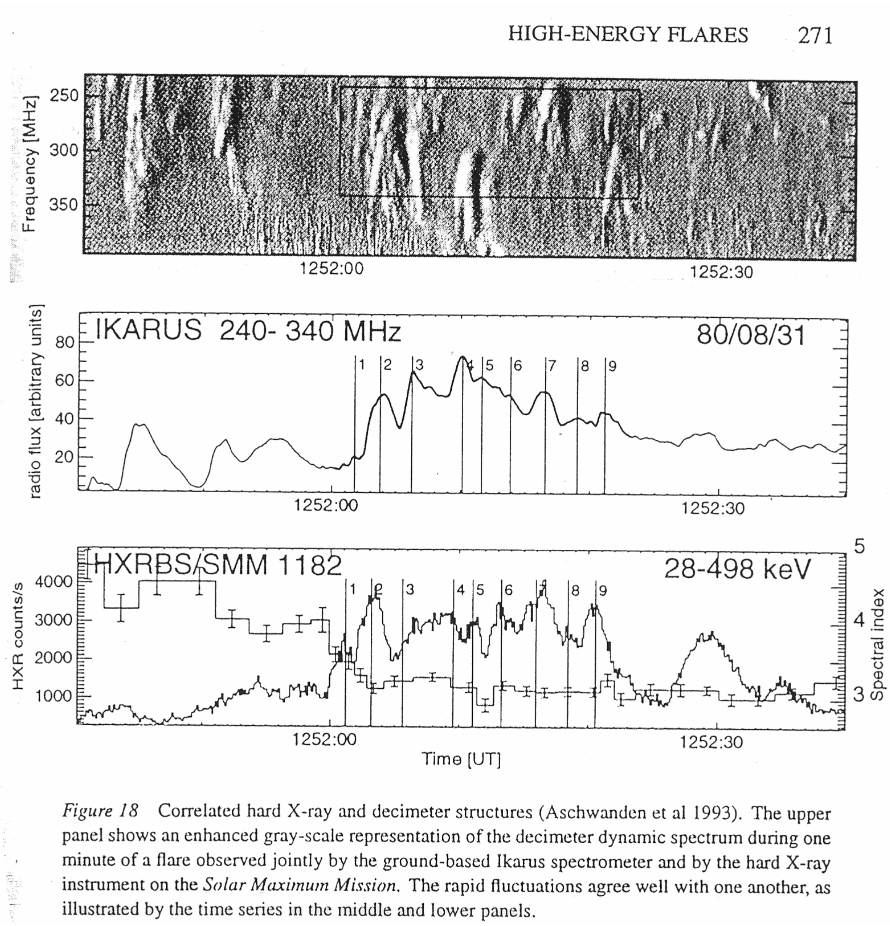

Figure 3.19: Radio type III bursts correlate well with hard X-rays since both emissions are caused by the same particle populations. Radio emission traces the electron beams and hard X-rays are created when the beams collide with dense matter. (From Hudson & Ryan, 1995)

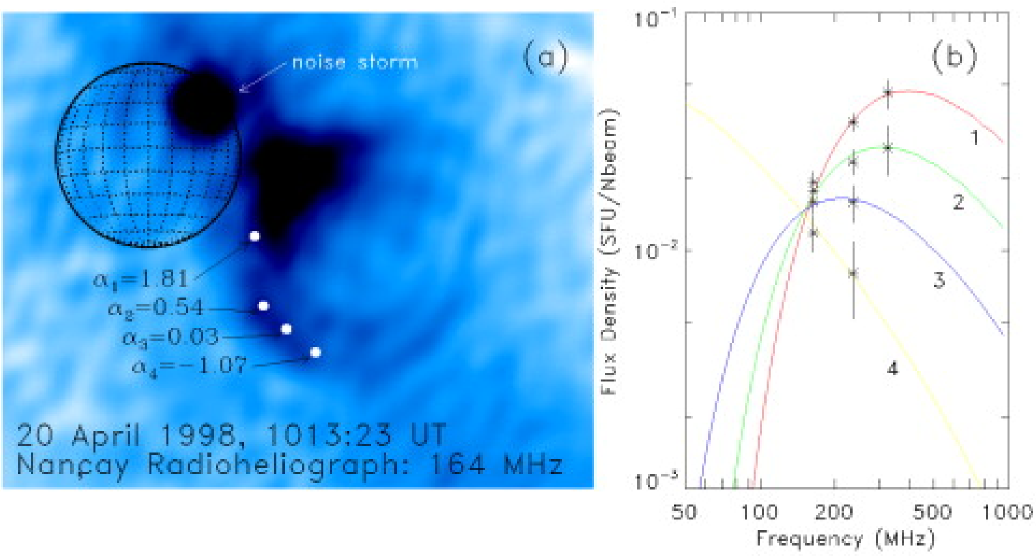

Figure 3.20: This is not plasma radiation! Emits at 164 MHz at heights over 4 $R_\odot \rightarrow$ synchrotron radiation $E_e \approx 0.5 - 5$ MeV, $B \approx 0.1$ G (Bastian et al., 2001)